Journal of Theoretical Biology **247** (2007) 672-686

The stochastic chemomechanics of the F_1-ATPase molecular motor

P. Gaspard and E. Gerritsma
Center for Nonlinear Phenomena and Complex Systems,
Université Libre de Bruxelles, Code Postal 231, Campus Plaine, B-1050 Brussels, Belgium

We report a theoretical study of the F_1-ATPase molecular rotary motor experimentally studied by R. Yasuda, H. Noji, M. Yoshida, K. Kinosita Jr., and H. Itoh [Nature **410**, 898 (2001)]. The motor is modeled as a stochastic process for the angle of its shaft and the chemical state of its catalytic sites. The stochastic process is ruled by six coupled Fokker-Planck equations for the biased diffusion of the angle and the random jumps between the chemical states. The model reproduces the experimental observations that the motor proceeds by substeps and the rotation rate saturates at high concentrations of adenosine triphosphate or at low values of the friction coefficient. Moreover, predictions are made about the dependence of the rotation rate on temperature, and about the behavior of the F_1 motor under the effect of an external torque, especially, in the regime of synthesis of adenosine triphosphate.

Keywords: molecular motor, F_1-ATPase, mechanochemical coupling, stochastic process, Arrhenius kinetics.

I. INTRODUCTION

F_1-ATPase is the hydrophilic part of the F_oF_1-ATPase also known as ATP synthase, which is an adenosine triphosphate (ATP) producing protein common to most living organisms [1]. *In vivo*, the two parts of ATP synthase, F_o and F_1, are attached to each other and mechanically coupled by the central γ-shaft. ATP synthesis occurs in natural systems when an ion gradient (commonly H^+, or Na^+ in some cases depending on the ATPase type) passes through the membrane embedded F_o part of the protein. The chemical ion gradient induces the rotation of F_o and the γ-shaft. The rotating γ-shaft creates a torque on the static F_1 part, which leads to a sequential conformational change of its $\alpha\beta$ sub-parts. F_1-ATPase is composed of three α and three β subunits spatially alternated and arranged around a central γ-shaft giving it a three-fold symmetry [2]. This complex protein mechanism leads to ATP catalysis when substrates adenosine diphosphate (ADP) and inorganic phosphate (P_i) are bound to one of the three β catalytic sites [3]. This phenomenon is crucial in the energetic metabolism of the cell since it provides the energy necessary for the endothermic ATP synthesis reaction [4].

When the F_1 part is not coupled to the F_o part, it can work in the opposite direction hydrolysing ATP and driving the rotation of the γ-shaft, as a nanomotor called F_1-ATPase. When ATP binds to the F_1-ATPase it induces a conformational change of the catalytic β subunit and its surrounding, which enforces a torque on the γ-shaft. Several experiments have demonstrated the rotary hydrolysis of ATP by F_1-ATPase. Early experiments by Kinosita and coworkers have shown that the rotation of the γ-shaft with an actin filament attached to it proceeds in steps of 120° [5]. Thereafter, a colloidal bead was attached to the γ-shaft, which reduced the friction and revealed substeps in each 120° step [6, 7]. These experiments showed that the ATP binding to F_1-ATPase forces the γ-shaft in a primary 80°-90° rotation and that the release of products of ATP hydrolysis to ADP and P_i induces a secondary 40°-30° rotation. These experiments demonstrate unambiguously the coupling of the mechanical rotation with the protein chemical activity. Moreover, ATP synthesis by mechanically driven F_1-ATPase has been successfully achieved in the remarkable experiments reported in Ref. [17].

The F_1 motor has been modeled by Oster and Wang [8, 9] prior to the experiments of Ref. [6] revealing the substeps. More recently, Sun, Wang, and Oster proposed a quantitative model that accounts for these substeps [10]. This very complete model with 64 chemical states describes the mechanochemical behavior of the F_1 motor as a crankshaft escapement that converts the elastic bending of the β subunits into the rotation of the γ-shaft. On the other hand, a model based on enzyme kinetics and Langevin dynamics was proposed by Liu *et al.* [11] and a model including the different conformations of the β subunits was developed by Gao *et al.* [12].

Nevertheless, many questions are still open concerning the coupling between chemistry and mechanics in the F_1 motor. First of all, the dependence on temperature of its kinetics is still poorly understood, albeit this dependence is crucial to determine the activation barriers. Besides, little is quantitatively known about the response of the F_1 motor to an external torque and the transition to the regime of ATP synthesis. This is important in order to know whether the motor works with tight or loose coupling between its chemical and mechanical features [18]. Moreover, a

question of fundamental interest is to understand the efficiency of the F_1 motor and, more generally, its nonequilibrium thermodynamics.

The purpose of the present paper is to address these issues in a stochastic model of the F_1 motor with six chemical states and the continuous angle of rotation for the γ-shaft. This model is based on detailed structural and kinetic information [6] and follows the principles of the "binding-change mechanism" of Paul D. Boyer [4] applied to the F_1 motor. As we will show, this six-state chemomechanical model is able to reproduce the main experimental observations of Ref. [6], in spite of the simplification with respect to the 64-state model by Sun, Wang, and Oster [10]. Thanks to this model, we make predictions about: the speed-up of the motor as temperature increases; the dependence of its behavior on an external torque; the transition to the regime of ATP synthesis; and its efficiency as a function of the external torque. *In vivo*, this external torque is due to the driving by the F_o proton turbine. *In vitro*, it is induced by a rotating magnetic field acting on a bead attached to the γ-shaft [17]. This allows us to answer several important questions concerning the coupling between the mechanical motion induced by the external torque and the chemistry of the motor, in particular, during ATP synthesis.

It is *a priori* surprising that nanomachines such as the F_1 motor can generate coordinated motion in spite of the thermal and molecular fluctuations which are important at the nanoscale. Indeed, disordered Brownian motion may affect larger particles of a few micrometers. Therefore, protein mechanics and chemistry are also stochastic phenomena since the characteristic length scales of these systems are between 10-100 nm. This stochastic behavior is well observed in the rotation angle of the γ-shaft which undergoes small fluctuations due to the random collisions with solvent molecules. The chemical activity is also stochastic since the arrivals of substrate ATP or ADP and P_i are random events in time. In our model, the rotation of the γ-shaft is described as a rotary Brownian motion in the free-energy potentials of six chemical states which are determined phenomenologically using the experimental data of Ref. [6]. The random transitions between these chemical states are described as Markovian stochastic processes. This overall stochastic process can be numerically simulated by Gillespie's algorithm [14–16]. Our model satisfies the principle of detailed balance at thermodynamic equilibrium. Directed motion becomes possible as soon as the motor is driven out of equilibrium by chemical or mechanical energies. The sources of these energies are respectively the nonequilibrium chemical concentrations of ATP, ADP and P_i, and the external torque. If the driving is far enough from equilibrium, the directed motion dominates the fluctuating motion.

One of the specificities of our model is that its reaction rates are established on the basis of Arrhenius' law of chemical kinetics. Accordingly, each reaction proceeds via some transition state in the energy landscape and is characterized by an activation energy. The thermal activation above the energy barrier determines the rate of each reaction. The fact that the activation energies are non-negative imposes important theoretical constraints to the model. By specifying the activation energies according to Arrhenius' law, our model is able to make predictions about the behavior of the F_1 motor over a whole range of temperatures and to explain the speed-up of rotation as temperature increases. For this aim, it is essential to determine the energy landscape of the transition states as well as the chemical states, which they connect. The energy landscape of both the chemical and transition states describes in a fundamental way the cooperativity among the subunits composing the F_1 motor and this, according to Boyer's binding-change mechanism [4]. In particular, the reactions of ATP binding and product release must be correlated with specific angles of the γ-shaft, which is indeed achieved in our model.

Furthermore, we study the response of the F_1 motor to an external torque and, in particular, its efficiency measured by the number of ATP molecules which are consumed or produced per revolution. This allows us to predict that the chemomechanical coupling is tight or loose depending on the external torque [18].

The paper is organized as follows. The model is presented in Sec. II. The dependence of the rotation on ATP concentration is studied in Sec. III. The effects of friction and temperature are discussed in Sec. IV. In Sec. V, we describe the behavior of the motor in the presence of the products of ATP hydrolysis. Section VI is devoted to the effects of an external torque on the motor. Conclusions are drawn in Sec. VII.

II. THE SIX-STATE MODEL OF THE F_1-ATPase MOTOR

A. The chemistry of F_1-ATPase

The rotation of the F_1-ATPase motor is driven by the hydrolysis of adenosine triphosphate (ATP) into adenosine diphosphate (ADP) and inorganic phosphate (P_i):

$$\mathrm{ATP} \rightleftharpoons \mathrm{ADP} + \mathrm{P_i} \tag{1}$$

The equilibrium standard Gibbs free energy of hydrolysis is $\Delta G^0 = -30.5$ kJ/mol $= -7.3$ kcal/mol $= -50$ pN nm so that the equilibrium concentrations satisfy

$$\frac{[\mathrm{ATP}]_{\mathrm{eq}}}{[\mathrm{ADP}]_{\mathrm{eq}}[\mathrm{P_i}]_{\mathrm{eq}}} = \exp\frac{\Delta G^0}{k_{\mathrm{B}}T} \simeq 4.89\ 10^{-6}\ \mathrm{M}^{-1} \tag{2}$$

at the temperature of 23 degrees Celsius and pH 7. This shows that the products of ATP hydrolysis are favored. The motor is in a nonequilibrium state if the concentrations do not satisfy Eq. (2), whereupon its mean rotation becomes possible. We notice that the mean rotation rate should vanish at equilibrium.

In the present paper, we consider the $\mathrm{F_1}$-ATPase molecular motor built by Kinosita and coworkers [6]. Their $\mathrm{F_1}$ protein complex is derived from the thermophilic *Bacillus* PS3. On the one hand, the stator has a diameter of about 10 nm and is composed of the protein hexamer $(\alpha\beta)_3$ which forms a barrel for the rotation of the γ-shaft. On the other hand, a colloidal gold bead of diameter 40 nm is attached to the γ-shaft [6]. This $\mathrm{F_1}$-ATPase molecular motor is schematically depicted in Fig. 1.

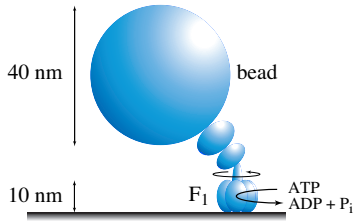

FIG. 1: Schematic representation of the $\mathrm{F_1}$ motor fixed on a surface and with a bead attached to its shaft, as considered in the experiments of Ref. [6].

The hydrolysis of ATP happens in the catalytic sites of the three β subunits of the stator. Upon ATP binding, the γ-shaft rotates by 80°-90°, which is the first substep of the rotation. After ATP hydrolysis, the release of the products ADP and $\mathrm{P_i}$ occur, and the γ-shaft further rotates by 40°-30°, which is the second substep of the rotation. During the ATP hydrolysis cycle of the motor, the sequence of reactions is coupled to the unidirectional rotation of the γ-shaft. The reversed rotation is accompanied by ATP synthesis [17]. We notice that the directionality of the motor finds its origin in the chirality of the $\mathrm{F_1}$ protein structure.

Each catalytic site of the three β subunits can be empty $\emptyset$ or occupied by either ATP, ADP·$\mathrm{P_i}$, ADP, $\mathrm{P_i}$, or excited states of these species. In this respect, the total number of possible chemical states is very large. The model by Oster and coworkers [8–10] considers the four occupancy states $\{\emptyset$, ATP, ADP·$\mathrm{P_i}$, ADP$\}$ for each β subunits, resulting in a total of $4^3 = 64$ possible states. However, it turns out that only a few among these states are actually observed in the experiments [6]. *A priori*, the motor could work on the basis of either a uni-site, a bi-site, or a tri-site mechanism whether at most one, two, or three β subunits are occupied during the cycle. The uni-site mechanism does not seem to occur with an important probability, except at extremely low ATP concentrations where the rotation becomes irregular [19]. At higher ATP concentrations, a switching between the bi-site and the tri-site cycles is possible as represented in Fig. 2. We have chosen to identify together the states of the bi- and tri-site mechanisms. This is justified because their distinction is difficult to observe experimentally [6]. This simplifying assumption is supported by the fact that the ATP binding is the driving event of the process, as also supposed in the "binding-change mechanism" of Paul D. Boyer [4].

The experiments of Ref. [6] have clearly revealed one reaction (i.e., ATP binding) during the first 80°-90° substep and two reactions during the other 40°-30° substep, and this for each one of the three 120° steps. This suggests nine chemical states over the cycle of the motor. In our model, the two successive chemical states during the 40°-30° substep are lumped into a single state, which leads to a model with a total of six chemical states. Accordingly, the model supposes that the products ADP and $\mathrm{P_i}$ are released together. This simplification still allows us to reproduce the observed substeps in the mechanical rotation, as well as the main features of the motor. In summary, our model is based on the reaction network with the following six chemical states $\sigma = 1, 2, ..., 6$:

$$\begin{array}{ccccccc} \cdots & \rightleftharpoons & 1 = (\emptyset, x, \mathrm{ADP}) & \rightleftharpoons & 2 = (\mathrm{ATP}, x, \mathrm{ADP}) & & \\ & \rightleftharpoons & 3 = (\mathrm{ADP}, \emptyset, x) & \rightleftharpoons & 4 = (\mathrm{ADP}, \mathrm{ATP}, x) & & \\ & \rightleftharpoons & 5 = (x, \mathrm{ADP}, \emptyset) & \rightleftharpoons & 6 = (x, \mathrm{ADP}, \mathrm{ATP}) & \cdots & \end{array} \tag{3}$$

where x stands an empty site $\emptyset$ or a site occupied by ADP. Here, we mean by ADP any state in which adenosine is present in the catalytic site and which is not the state during ATP binding (see Fig. 2).

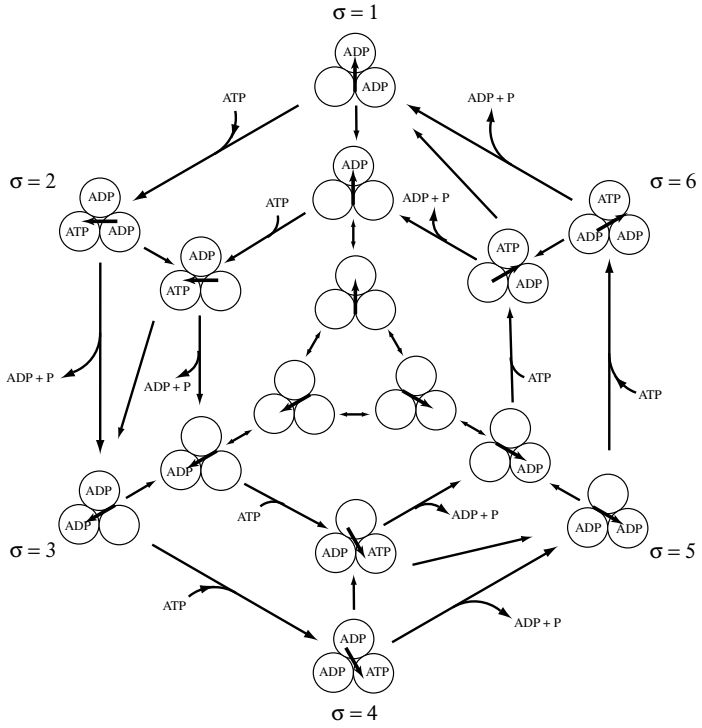

FIG. 2: The motor cycle and its possible states. The inner ring contains three states with empty sites and three possible shaft angles. The second and third rings represent the motor cycles based on the bi- and tri-site mechanisms. The intermediate state which is here denoted ADP is either an excited state ATP* of ATP, ADP·P_i, or ADP alone in the corresponding catalytic site [6]. P denotes inorganic phosphate.

B. The mechanics of F_1-ATPase

In each chemical state σ, the shaft of the motor is submitted to an internal torque caused by some free-energy potential $U_\sigma(\theta)$ which depends on the angle θ. We notice that the experiment is carried out at constant atmospheric pressure so that we are here talking about Gibbs free energies. Moreover, the molecular fluctuations induce a random torque $\tau_{\rm fluct}(t)$ due to the environment. The motion of this angle is thus described by an overdamped Langevin-type equation

$$\zeta \, \frac{d\theta}{dt} = -\frac{\partial U_\sigma}{\partial \theta} + \tau_{\rm ext} + \tau_{\rm fluct}(t) \tag{4}$$

where $\tau_{\rm ext}$ is some external torque. The fluctuating torque is taken as a Gaussian white noise related to the friction coefficient ζ according to the fluctuation-dissipation theorem:

$$\langle \tau_{\rm fluct}(t) \rangle \;=\; 0 \tag{5}$$

$$\langle \tau_{\rm fluct}(t) \tau_{\rm fluct}(t') \rangle \;=\; 2\, k_{\rm B} T \, \zeta \, \delta(t-t') \tag{6}$$

The friction is due to the viscosity $\eta = 10^{-9}$ pN s nm^{-2} of the water in which the bead or the filament attached to the shaft moves. The contribution from the friction internal to the motor is neglected. Accordingly, the friction coefficient is given by:

$$\zeta = 8\pi\eta r^3 + 6\pi\eta r x^2 \tag{7}$$

for a bead of radius r attached off axis with its center at the distance x from the rotation axis [6, 20]; by

$$\zeta = 16\pi\eta r^3 + 6\pi\eta r x_1^2 + 6\pi\eta r x_2^2 \tag{8}$$

for bead duplex of radii r at distances x_1 and x_2 from the rotation axis [6]; and by

$$\zeta = \frac{4\pi}{3} \frac{\eta l^3}{\ln \frac{l}{2r} + \gamma_{\rm r}} \tag{9}$$

for an actin filament supposed to be a cylinder of length l and radius r attached perpendicularly by one of its ends to the shaft with $\gamma_{\rm r} = -0.55 \pm 0.11$ [21].

C. Coupling the chemistry to the mechanics

During the time evolution of the motor, reactive events happen randomly. The chemical state σ and its associated potential U_σ change accordingly at each one of these random events. The mechanical motion of the shaft is thus coupled to the chemical reaction in such chemomechanical processes. The state of the system is described by the probability density $p_\sigma(\theta,t)$ to find the motor in the chemical state σ with its shaft forming the angle θ at time t. The time evolution of the probability densities is ruled by a set of coupled Fokker-Planck equations including terms for the description the random jumps between the discrete chemical states σ:

$$\partial_t\, p_\sigma(\theta,t) + \partial_\theta\, J_\sigma(\theta,t) = \sum_{\rho,\sigma'(\neq\sigma)} \left[p_{\sigma'}(\theta,t)\, W_{\rho,\sigma'\to\sigma}(\theta) - p_\sigma(\theta,t)\, W_{-\rho,\sigma\to\sigma'}(\theta)\right] \tag{10}$$

with the probability current densities

$$J_\sigma = -D\,\partial_\theta\, p_\sigma + \frac{1}{\zeta}\left(-\partial_\theta U_\sigma + \tau_{\rm ext}\right) p_\sigma \tag{11}$$

given in terms of the diffusion coefficient

$$D = \frac{k_{\rm B}T}{\zeta} \tag{12}$$

and the deterministic torque $-\partial_\theta U_\sigma + \tau_{\rm ext}$ which biases the random rotation [13]. The index ρ denotes the different chemical reactions undergone by the motor. The left-hand sides of Eqs. (10) describe the mechanics and their right-hand sides the reactions.

Since there are six chemical states and two chemical reactions (ATP binding and release of the products) with their corresponding reversed reactions, the model is defined by the following six coupled Fokker-Planck equations:

$$\begin{aligned}
\partial_t\, p_{2i+1} + \partial_\theta\, J_{2i+1} \;=\; & -\left[W_+\left(\theta-\frac{2\pi i}{3}\right) + \tilde{W}_-\left(\theta-\frac{2\pi i}{3}\right)\right] p_{2i+1} \\
& + W_-\left(\theta-\frac{2\pi i}{3}\right) p_{2i+2} + \tilde{W}_+\left(\theta-\frac{2\pi i}{3}\right) p_{2i}
\end{aligned} \tag{13}$$

$$\begin{aligned}
\partial_t\, p_{2i+2} + \partial_\theta\, J_{2i+2} \;=\; & -\left[W_-\left(\theta-\frac{2\pi i}{3}\right) + \tilde{W}_+\left(\theta-\frac{2\pi(i+1)}{3}\right)\right] p_{2i+2} \\
& + W_+\left(\theta-\frac{2\pi i}{3}\right) p_{2i+1} + \tilde{W}_-\left(\theta-\frac{2\pi(i+1)}{3}\right) p_{2i+3}
\end{aligned} \tag{14}$$

with $i = 0, 1, 2$. We make the identifications $p_0 = p_6$ and $p_7 = p_1$. The probability current densities $J_\sigma(\theta,t)$ are defined by Eq. (11) for each given state $\sigma = 1, 2, ..., 6$.

The transition rates obey Arrhenius' law of kinetics in terms of the activation energies of each reaction. These activation energies are given by the difference between the energy of the transition state of the corresponding reaction and the energy of the potential well of the initial state. The potentials of both the wells and the transition states depend on the angle θ of the shaft. The potential of the transition state of ATP binding is denoted by $U_1^\ddagger(\theta) = U^\ddagger(\theta)$ and the one for the release of the products ADP and $\rm P_i$ by $U_2^\ddagger(\theta) = \tilde{U}^\ddagger(\theta)$ for the first β subunit. The potential of the state where the first β subunit is empty is denoted by $U_1(\theta) = U(\theta)$ and by $U_2(\theta) = \tilde{U}(\theta)$ if it is occupied. The potentials of the other states are obtained by 120° rotations according to:

$$U_{2i+1}(\theta) \;=\; U\left(\theta-\frac{2\pi i}{3}\right) \tag{15}$$

$$U_{2i+2}(\theta) \;=\; \tilde{U}\left(\theta-\frac{2\pi i}{3}\right) \tag{16}$$

$$U^\ddagger_{2i+1}(\theta) \;=\; U^\ddagger\left(\theta-\frac{2\pi i}{3}\right) \tag{17}$$

$$U^\ddagger_{2i+2}(\theta) \;=\; \tilde{U}^\ddagger\left(\theta-\frac{2\pi i}{3}\right) \tag{18}$$

TABLE I: Table showing the different chemical states $\sigma = 1, 2, ..., 6$, their free-energy potentials $U_\sigma(\theta)$, the forward and backward transition rates and the corresponding transition states by their potentials $U^\ddagger_\sigma(\theta)$.

state σ	potential $U_\sigma(\theta)$	transition state	forward	transition rate	backward	transition rate
		$\tilde{U}^\ddagger(\theta)$	$\downarrow$	$\tilde{W}_+(\theta)$	$\uparrow$	$\tilde{W}_-(\theta)$
1	$U(\theta)$		1		1	
		$U^\ddagger(\theta)$	$\downarrow$	$W_+(\theta)$	$\uparrow$	$W_-(\theta)$
2	$\tilde{U}(\theta)$		2		2	
		$\tilde{U}^\ddagger\left(\theta - \frac{2\pi}{3}\right)$	$\downarrow$	$\tilde{W}_+\left(\theta - \frac{2\pi}{3}\right)$	$\uparrow$	$\tilde{W}_-\left(\theta - \frac{2\pi}{3}\right)$
3	$U\left(\theta - \frac{2\pi}{3}\right)$		3		3	
		$U^\ddagger\left(\theta - \frac{2\pi}{3}\right)$	$\downarrow$	$W_+\left(\theta - \frac{2\pi}{3}\right)$	$\uparrow$	$W_-\left(\theta - \frac{2\pi}{3}\right)$
4	$\tilde{U}\left(\theta - \frac{2\pi}{3}\right)$		4		4	
		$\tilde{U}^\ddagger\left(\theta - \frac{4\pi}{3}\right)$	$\downarrow$	$\tilde{W}_+\left(\theta - \frac{4\pi}{3}\right)$	$\uparrow$	$\tilde{W}_-\left(\theta - \frac{4\pi}{3}\right)$
5	$U\left(\theta - \frac{4\pi}{3}\right)$		5		5	
		$U^\ddagger\left(\theta - \frac{4\pi}{3}\right)$	$\downarrow$	$W_+\left(\theta - \frac{4\pi}{3}\right)$	$\uparrow$	$W_-\left(\theta - \frac{4\pi}{3}\right)$
6	$\tilde{U}\left(\theta - \frac{4\pi}{3}\right)$		6		6	

with $i = 0, 1, 2$, as shown in Table I.

The transition rates are therefore given by:

$$W_+(\theta) = k_0\,[\mathrm{ATP}]\,\exp\left\{-\beta\left[U^\ddagger(\theta) - U(\theta) - G^\circ_{\mathrm{ATP}}\right]\right\} \tag{19}$$

$$W_-(\theta) = k_0\,\exp\left\{-\beta\left[U^\ddagger(\theta) - \tilde{U}(\theta)\right]\right\} \tag{20}$$

$$\tilde{W}_+(\theta) = \tilde{k}_0\,\exp\left\{-\beta\left[\tilde{U}^\ddagger(\theta) - \tilde{U}\left(\theta + \frac{2\pi}{3}\right)\right]\right\} \tag{21}$$

$$\tilde{W}_-(\theta) = \tilde{k}_0\,[\mathrm{ADP}]\,[\mathrm{P_i}]\,\exp\left\{-\beta\left[\tilde{U}^\ddagger(\theta) - U(\theta) - G^\circ_{\mathrm{ADP}} - G^\circ_{\mathrm{P_i}}\right]\right\} \tag{22}$$

with $\beta = 1/k_{\mathrm{B}}T$. Equations (19)-(22) represent, respectively, the transition rates of binding and unbinding of ATP, and of unbinding and binding of ADP and $\mathrm{P_i}$ to the first β subunit. The other transitions rates are obtained by 120° rotations as shown in Table I. As a consequence, the system ruled by the six coupled Fokker-Planck equations has threefold symmetry because of the threefold structure of $\mathrm{F_1}$-ATPase. We notice that the system does not have any reflection symmetry, which is to be attributed to the chirality of the supramolecular architecture of the $\mathrm{F_1}$ molecular motor and is essential for its unidirectional rotation in the presence of its chemical fuel. In establishing Eqs. (19)-(22), it has been supposed that the activation energy is given by the potential of the transition state minus the sum of the potentials of the reactants. For the transition rates (20) and (21), the reactions are unimolecular so that the reactant is the sole protein complex formed by the motor with bounded substrates. For the transition rates (19) and (22), the reactions are bi- and tri-molecular so that there are respectively two and three reactants including the motor and smaller molecules which are present in the solvent surrounding the motor with some concentration. The free-energies of these molecules are equal to their chemical potentials which depend on their concentration according to

$$\mu_{\mathrm{X}} = G_{\mathrm{X}} = G^0_{\mathrm{X}} + k_{\mathrm{B}}T\ln[\mathrm{X}] \tag{23}$$

with X=ATP, ADP, or $\mathrm{P_i}$. G^0_{X} is a reference free-energy corresponding to one mole per liter.

The free-energy potentials of the wells are fitted to the experimental data (see Fig. 3). Figure 5 of of Ref. [6] depicts the probability densities of finding the shaft at some angle θ. At the low ATP concentration of 2 μM, the motor is waiting for ATP binding so that the probability density can be used to determine the free-energy potential $U(\theta)$ of the motor with an empty β subunit. It is here supposed that the fluctuations of the angle θ are in quasi equilibrium so that their probability density should be given by Boltzmann factor $\exp\left[-U(\theta)/k_{\mathrm{B}}T\right]$, allowing the determination of the potential. At the high ATP concentration of 2 mM, the motor is waiting for the release of the products so that the probability density determines the free-energy potential $\tilde{U}(\theta)$ of the motor with an occupied β subunit. In this way, the free-energy potentials can be fitted to experimental data and are given by:

$$U(\theta) = a + b\,\cos\theta + c\,\cos 3\theta \tag{24}$$

$$\tilde{U}(\theta) = \tilde{a} + \tilde{b}\,\cos\left(\theta - \frac{\pi}{2}\right) + \tilde{c}\,\cos\left[3\left(\theta - \frac{\pi}{2}\right)\right] \tag{25}$$

with the constants of Table II. The potential $\tilde{U}(\theta)$ has its minimum 20 pN nm above the minimum of $U(\theta)$ as in Ref. [6]. The potentials (24) and (25) describe the global effect of the hexamer $(\alpha\beta)_3$ onto the γ-shaft and, thus, take into account the cooperativity among the different subunits.

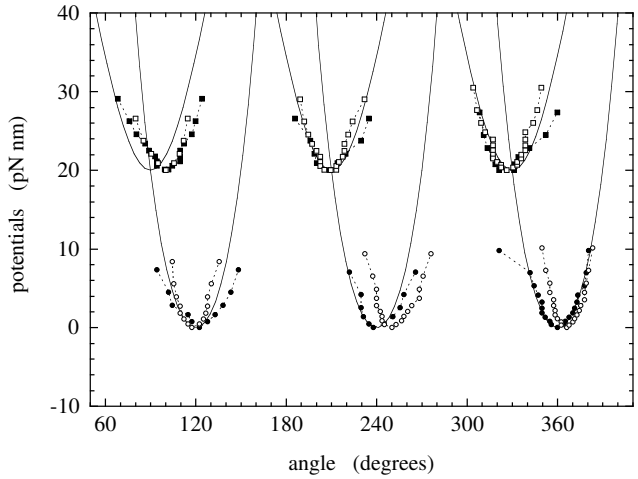

FIG. 3: The free-energy potentials of the chemical states fitted to the experimental data given in Fig. 5 of Ref. [6]. The lower curves give the potentials $U_1(\theta) = U(\theta)$, $U_3(\theta) = U(\theta - 2\pi/3)$, and $U_5(\theta) = U(\theta - 4\pi/3)$. The upper curves give the potentials $U_2(\theta) = \tilde{U}(\theta)$, $U_4(\theta) = \tilde{U}(\theta - 2\pi/3)$, and $U_6(\theta) = \tilde{U}(\theta - 4\pi/3)$.

The potentials of the transition states are given by:

$$U^{\ddagger}(\theta) = E^{\ddagger} + a^{\ddagger}\,(1 - \cos\theta) \tag{26}$$

$$\tilde{U}^{\ddagger}(\theta) = \tilde{E}^{\ddagger} + \tilde{a}^{\ddagger}\left[1 - \cos\left(\theta + \frac{\pi}{6}\right)\right] \tag{27}$$

with the constants of Table II. We have assumed that their minimum is located at the minimum of the potential well of the corresponding reaction as shown in Fig. 4. The width of the bottlenecks are taken to avoid spurious minima in the activation barriers. The activation energies $E^{\ddagger}$ and $\tilde{E}^{\ddagger}$ have been taken in order that all the activation energies in Eqs. (19)-(22) are non-negative, as required by Arrhenius' law. There is an activation barrier for the release of the products and it is assumed that ATP binding has a negligibly small barrier.

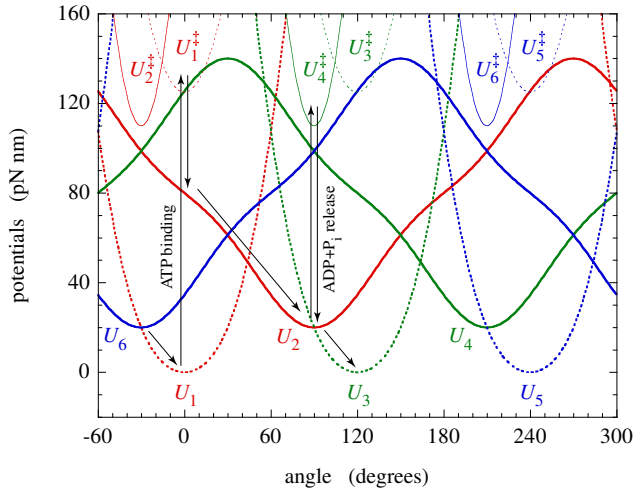

FIG. 4: The potentials of the chemical states $U_\sigma(\theta)$ and of the transition states $U_\sigma^{\ddagger}(\theta)$ with a schematic representation of the transitions between them during the motor cycle. In this diagram, the relative level of the potentials is fixed by Eqs. (15)-(18) with (24)-(27) and is not indicative of the actual reaction barriers.

The reaction constants k_0 and $\tilde{k}_0$ have been fitted to reproduce the Michaelis-Menten dependence of the mean rotation rate as a function of ATP concentration in Fig. 3 of Ref. [6].

TABLE II: Values of the coefficients in the potentials of the chemical states and transition states, and the transition rates.

coefficient	value	units
a	272.5	pN nm
b	-291.6	pN nm
c	19.1	pN nm
$\tilde{a}$	80	pN nm
$\tilde{b}$	-52.5	pN nm
$\tilde{c}$	-7.5	pN nm
$E^\ddagger$	125	pN nm
$a^\ddagger$	360	pN nm
$\tilde{E}^\ddagger$	110	pN nm
$\tilde{a}^\ddagger$	900	pN nm
$G^0_{\rm ATP}$	125	pN nm
$G^0_{\rm ADP}$	75	pN nm
$G^0_{\rm P_i}$	0	pN nm
k_0	$4.1\ 10^7$	s^{-1}
$\tilde{k}_0$	$4.0\ 10^{12}$	s^{-1}

The constant $G^0_{\rm ADP} + G^0_{\rm P_i}$ have been fitted to reproduce the dependence of the mean rotation rate as a function of friction in Fig. 2 of Ref. [6]. The value of the constant $G^0_{\rm ATP}$ follows from the standard Gibbs free-energy of ATP hydrolysis and the principle of detailed balance at the thermodynamic equilibrium, as shown in Appendix A.

The method of stochastic simulations of the model is explained in Appendix B.

III. THE EFFECTS OF ATP

In this section, we consider the motor in the presence of its fuel supposing that the products of ATP hydrolysis are quickly evacuated. Accordingly, we take $[{\rm ADP}][{\rm P_i}] = 0$. A bead of diameter $d = 40$ nm is attached to the γ-shaft. The center of the bead is supposed at the distance $x = 0.25d$ from the rotation axis. The friction coefficient is given by Eq. (7) with the bead radius $r = d/2$. The temperature is of 23 degrees Celsius.

The studied property is the rotation of the γ-shaft as a function of ATP concentration, as depicted in Fig. 5. The rotation is characterized by the mean angular velocity $V = (2\pi)^{-1}\langle d\theta/dt\rangle$, which is the mean rotation rate in revolutions per second. The solid line gives the result of the numerical simulation of the present model, which is compared with the experimental data in Fig. 3 of Ref. [6]. The agreement between both has been used to fit the parameters of model as explained here above.

We notice that the model reproduces the Michaelis-Menten dependence of the rotation rate on the ATP concentration. The mean angular velocity fits with the following Michaelis-Menten kinetics

$$V \simeq \frac{V_{\rm max}\,[{\rm ATP}]}{[{\rm ATP}] + K_{\rm M}} \tag{28}$$

The maximum velocity $V_{\rm max} = 131.1 \pm 1.5$ rev/s and the Michaelis-Menten constant $K_{\rm M} = 16.3 \pm 0.4$ μM are in agreement with the experimental values $V_{\rm max} = 129 \pm 9$ rev/s and $K_{\rm M} = 15 \pm 2$ μM [6].

The Michaelis-Menten kinetics reveals a transition between two regimes. At low ATP concentration, the mean rotation rate is proportional to the ATP concentration, $V \simeq V_{\rm max}[{\rm ATP}]/K_{\rm M}$. The rotation is limited by the rarity of ATP molecules in the solvent surrounding the motor. The motor spends most of its time waiting for the arrival of ATP molecules. Accordingly, the constant of proportionality of the velocity $V_{\rm max}/K_{\rm M}$ depends on the reaction constant k_0 of ATP binding. At high ATP concentration, the mean rotation rate saturates at the maximum velocity $V \simeq V_{\rm max}$. In this regime, the rotation is limited by the release of the products ADP and $\rm P_i$ so that the maximum velocity $V_{\rm max}$ depends on the other reaction constant $\tilde{k}_0$.

Figure 6 depicts several stochastic trajectories of the angle $\theta(t)$ of the γ-shaft as a function of time t, as simulated by the model. The angle of the shaft is counted in terms of the number of revolutions $\theta/2\pi$. Moreover, horizontal

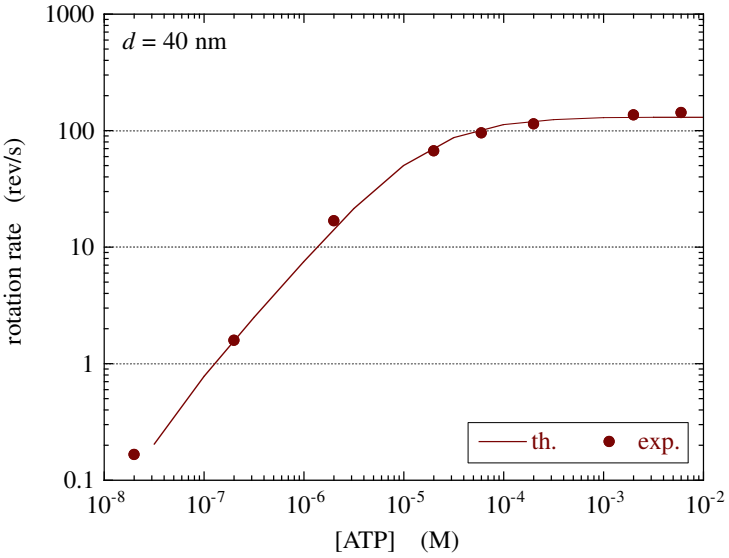

FIG. 5: Mean rotation rate of the γ-shaft of the F_1 motor in revolutions per second, versus the ATP concentration [ATP] in mole per liter for $[ADP][P_i] = 0$. The diameter of the bead is $d = 40$ nm. The temperature is of 23 degrees Celsius. The external torque is zero. The circles are the experimental data [6]. The solid line is the result of the present model.

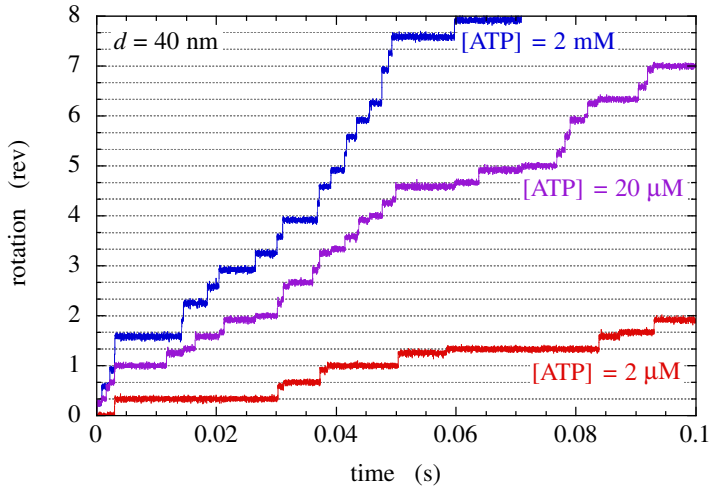

FIG. 6: Stochastic trajectories of the rotation of the γ-shaft of the F_1 motor. The number of revolutions $\theta(t)/2\pi$ is plotted versus time t in seconds for [ATP] = 2 μM, 20 μM, 2 mM, and $[ADP][P_i] = 0$. The diameter of the bead is $d = 40$ nm. The temperature is of 23 degrees Celsius. The external torque is zero. This figure is to be compared with Fig. 4 of Ref. [6].

lines are plotted in Fig. 6 at each third of a revolution in order to see the 120° steps in the rotation. For a bead of diameter $d = 40$ nm, Fig. 6 shows that the rotation proceeds in steps and substeps. The aforementioned transition in the Michaelis-Menten kinetics is directly related to the substeps in the rotation of the motor.

At the low ATP concentration of 2 μM, ATP binding is the limiting reaction so that, most of its time, the motor is waiting in the potential wells of the empty states around the angles $\theta = 0°$, 120°, and 240°, which are the minima of the potentials U_1, U_3, and U_5. The angle fluctuates due to its Brownian motion in these potential wells. The probability density of its fluctuations before the next jump are in quasi equilibrium with the Boltzmann distributions (A1). The rate of ATP binding is small and the release of the products is faster so that the dwell times are longer at the aforementioned angles when the motor is waiting for ATP binding.

At the high ATP concentration of 2 mM, ATP binding is faster than the release of the products so that the motor is instead waiting in the potential wells, U_2, U_4, and U_6, of the occupied states around the angles $\theta = 90°$, 210°, and 330°, as also seen in Fig. 6. In this case, the trajectories reveal the substeps of the release of the products because their dwell times are longer than for ATP binding.

For the intermediate ATP concentration of 20 μM, all the substeps at the six angles are observed.

These results show that the present model nicely reproduces the experimental features displayed in Fig. 4 of Ref. [6].

IV. THE EFFECTS OF FRICTION AND TEMPERATURE

A. Friction

Now, we study the dependence of the mean rotation rate on the viscous friction coefficient ζ. Here again, we suppose that $[\mathrm{ADP}][\mathrm{P_i}] = 0$. In the experiment of Ref. [6], the friction coefficient ζ is changed by attaching a bead, a bead duplex, or an actin filament of various size to the γ-shaft of the motor. The lowest friction is achieved with a single bead of diameter $d = 40$ nm and the largest with an actin filament of length $l = 1$-3 μm. The friction coefficient of these objects are given in Eqs. (7)-(9). The experimental data of Fig. 2 of Ref. [6] are plotted in our Fig. 7 and compared with the results of the numerical simulation of the model (solid line).

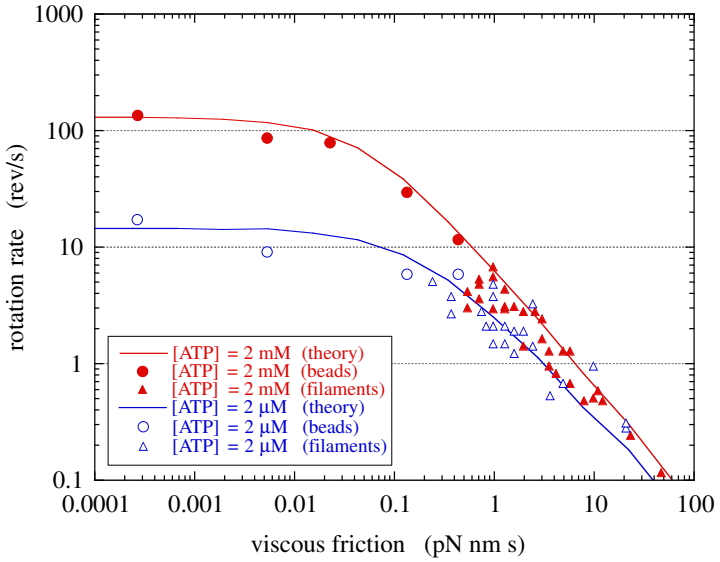

FIG. 7: The mean rotation rate V in revolutions per second versus the viscous friction coefficient ζ with a bead, a bead duplex, or a filament attached to the γ-shaft. The circles and triangles are the experimental data in Fig. 2 of Ref. [6] at [ATP] = 2 mM (filled circles and triangles) and [ATP] = 2 μM (open circles and triangles). The circles correspond to the single beads and bead duplexes, the triangles to the actin filaments. The solid lines are the results of the present model with $[\mathrm{ADP}][\mathrm{P_i}] = 0$ and the temperature of 23 degrees Celsius. The external torque is zero. The water viscosity is $\eta = 10^{-9}$ pN s nm^{-2} as elsewhere.

We notice that the mean rotation rate increases with ATP concentration as already explained in the previous section in terms of the Michaelis-Menten kinetics. Besides, we observe another transition between two regimes as the viscous friction is changed. The mean rotation rate shows a plateau at low friction and decreases at high friction.

At low friction, the mean rotation rate saturates. The reason is that the friction is low enough that it is no longer limiting the rotation. In this case, the stochastic rotary motion is relatively fast on the free-energy potentials of each chemical state, compared to the waiting in the potential wells before the next reaction. Therefore, we can speak of a *reaction-limited regime*. In this regime, the steps and substeps are well resolved.

At high friction, the stochastic rotary motion is slower on each potential than the reactions causing the jumps between the potentials. In this case, the rotation is limited by the friction instead of the reaction and we have a *friction-limited regime*.

Figure 8 depicts several stochastic trajectories of the motor with a bead of increasing size attached to the γ-shaft for [ATP] = 2 mM. The friction coefficient ζ thus increases with the diameter d according to Eq. (7). For beads with the small diameters of $d = 80$ and 160 nm, the friction is low so that the rotation is fast between the reactions, and the steps and substeps are clearly resolved in this reaction-limited regime. In contrast, the rotation on each potential is slower than the reactions at the higher friction of beads with the larger diameters of $d = 320$ and 640 nm or, equivalently, bead duplexes or actin filaments with the same friction coefficient ζ. Accordingly, the steps are smoothed out in this friction-limited regime.

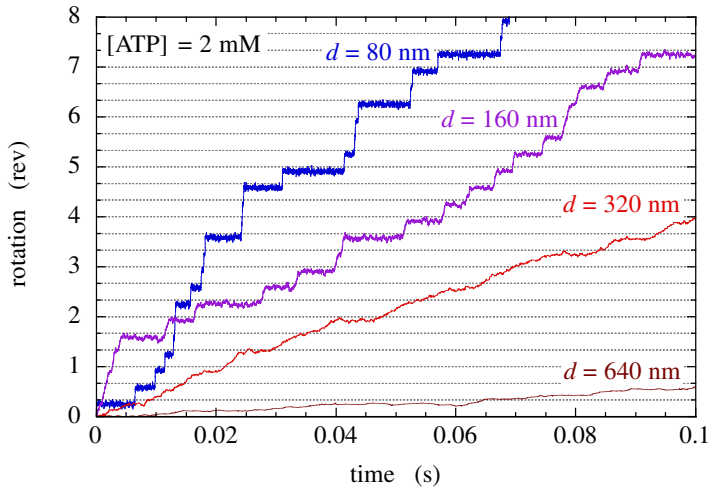

FIG. 8: Stochastic trajectories of the rotation of the γ-shaft of the F_1 motor with a single bead of diameter $d = 80$, 160, 320, and 640 nm, attached at the distance $x = 0.25d$ from the rotation axis or, equivalently, bead duplexes or actin filaments with the same friction coefficient ζ. The number of revolutions $\theta(t)/2\pi$ is plotted versus time t in second. The chemical concentrations are [ATP] = 2 mM and [ADP][P_i] = 0. The temperature is of 23 degrees Celsius. The external torque is zero. As already discussed in the previous section, we here again observe that the motor spends most of its time waiting for the release of the products around $\theta = 90°$, 210°, and 330°.

B. Temperature

Figure 9 depicts the mean rotation rate as a function of the inverse temperature. This simulation is carried out in the reaction-limited regime for a bead of diameter $d = 40$ nm and in the saturation regime of the Michaelis-Menten kinetics at the concentrations [ATP] = 0.01 M and [ADP][P_i] = 0. The mean rotation rate increases from about 105 revolutions per second at the temperature of 20 degrees Celsius up to 794 revolutions per second at the temperature of 50 degrees Celsius, following the Arrhenius behavior

$$V \simeq V_{\max} \sim \exp\left(-\frac{E_a}{k_B T}\right) \tag{29}$$

with the activation energy $E_a = 88.5$ pN nm. This is essentially the activation barrier for the release of the products since there is no barrier for ATP binding in the present model and the motor is cycling forward because [ADP][P_i] = 0.

In the present model, we notice that the binding of the products has an activation barrier of 8.8 pN nm and the release of ATP an activation barrier of 43.7 pN nm. However, these barriers do not manifest themselves under the condition [ADP][P_i] = 0 of the simulation of Fig. 9.

A discussion is here in order about the possibility that further barriers are revealed by experimental observations. Within the framework of the present model but for other values of the parameters, it is possible to take into account of a barrier for ATP binding. This energy barrier is fixed by the difference $E^\ddagger - G^0_{ATP}$ which is here vanishing for the values given in Table II. Beyond the framework of the present six-state model, further barriers are possible. If each one of the two reactions which are experimentally observed during the substeps of 40°-30° had its own activation barrier, a model with at least nine states should be envisaged. At higher temperatures, the proteins denaturate which could also contribute to special dependences of the mean rotation rate on temperature.

V. THE EFFECTS OF ADP AND P_i

The dependence of the mean rotation rate on the concentrations of the products ADP and P_i is also interesting to investigate. In the present model, the properties only depend on the combination [ADP][P_i].

Figure 10 shows the mean rotation rate versus the ADP concentration for [P_i] = 10^{-3} M and different ATP concentrations. We notice that the studied concentrations are very far from the thermodynamic equilibrium state where [ATP] = $4.89\,10^{-9}$[ADP] according to Eq. (2). However, they include the physiological conditions of [ATP] $\simeq$ 10^{-3} M, [ADP] $\simeq$ 10^{-4} M, and [P_i] $\simeq$ 10^{-3} M [20].

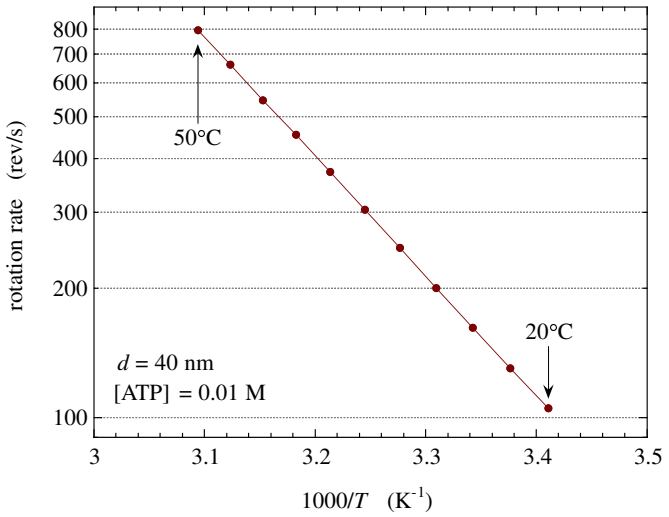

FIG. 9: The mean rotation rate V in revolutions per second versus the inverse $1000/T$ of the temperature T in Kelvin. The motor rotates a bead of diameter $d = 40$ nm. The concentrations are [ATP] = 0.01 M and [ADP][P_i] = 0. The activation energy of the seen Arrhenius behavior is $E_a = 88.5$ pN nm. The external torque is zero.

We see in Fig. 10 that the mean rotation rate increases with the ATP concentration as expected from its Michaelis-Menten dependence discussed in Section III. Furthermore, we observe that the mean rotation rate diminishes at high ADP concentration albeit it saturates at low ADP concentration. This confirms the expectation that the rotation is hindered by the presence of the products of ATP hydrolysis and shows that this happens if the concentrations of the products are sufficiently large. The curves of Fig. 10 can be approximated by

$$V \simeq \frac{V_{\max}\,([\mathrm{ATP}] - K_{\mathrm{eq}}[\mathrm{ADP}][\mathrm{P_i}])}{[\mathrm{ATP}] + K_{\mathrm{M}} + K_{\mathrm{P}}[\mathrm{ADP}][\mathrm{P_i}]} \tag{30}$$

which generalizes the Michaelis-Menten kinetics of Eq. (28). The numerator is taken such that the mean rotation rate vanishes at the equilibrium (2). As in Eq. (28), the maximum velocity is $V_{\max} = 131.1 \pm 1.5$ rev/s and the Michaelis-Menten constant $K_{\mathrm{M}} = 16.3 \pm 0.4$ μM. The equilibrium constant is given by $K_{\mathrm{eq}} = 4.89\ 10^{-6}\ \mathrm{M}^{-1}$ according to Eq. (2). The constant for the products takes the value $K_{\mathrm{P}} = 12.2 \pm 1.5\ \mathrm{M}^{-1}$. The dependence on [ADP][P_i] in the numerator is negligible because $K_{\mathrm{P}} \gg K_{\mathrm{eq}}$. We see in Fig. 10 that the formula (30) looses its validity as the ATP and concentrations exceed 10^{-3} M, but is otherwise in good agreement with the numerical results of the model.

VI. THE EFFECTS OF AN EXTERNAL TORQUE

The coupling between the mechanical and chemical properties of the F_1 motor plays an essential role if an external torque is applied to the γ-shaft. *In vivo*, the external torque is caused by the proton current that passes through the membrane embedded F_o part of F_oF_1-ATP synthase, the F_o part being mechanically coupled to the γ-shaft of the F_1-ATPase. *In vitro*, an external torque can be applied by electrical magnets driving a magnetic bead attached to the γ-shaft of the F_1 motor [17].

The external torque has the first effect of tilting the free-energy potentials into $U_\sigma(\theta) - \tau_{\mathrm{ext}}\theta$. The external torque can be either positive if applied in the direction of the mean rotation in the presence of chemical fuel or negative if opposed to this mean rotation. The resulting mean rotation rate is depicted in Fig. 11 as a function of the external torque in the presence of ADP and P_i and for different ATP concentrations. Figure 12 shows the corresponding numbers of ATP molecules which are produced per second by the system. The curves display several important features.

For negative torques opposing the mean motion, the rotation rate decreases from positive to negative values. The mean rotation rate vanishes at the critical negative value called the stalling torque. The stalling torque has a value between $\tau_{\mathrm{ext,stall}} \simeq -25$ pN nm and $\tau_{\mathrm{ext,stall}} \simeq -35$ pN nm, depending on the conditions. At lower values $\tau_{\mathrm{ext}} < \tau_{\mathrm{ext,stall}}$ of the external torque, the motor is mainly driven by the external torque and rotates backward, which can be explained by the tilting of the free-energy potentials seen in Fig. 13 (d) and (e). In this regime, the external torque drives the synthesis of ATP from ADP and P_i at the rate of about 50 ATP molecules per second in the given conditions, as seen in Fig. 12.

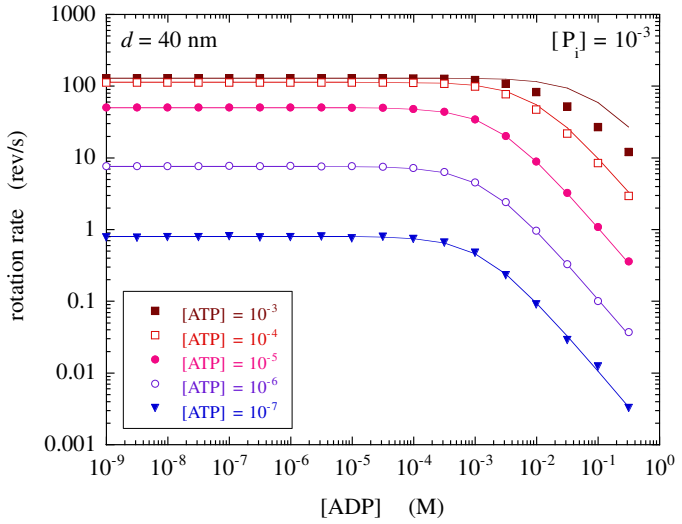

FIG. 10: The mean rotation rate V in revolutions per second versus the ADP concentration. The diameter of the bead is $d = 40$ nm. The concentrations of the other species are $[\mathrm{P_i}] = 10^{-3}$ M and $[\mathrm{ATP}] = 10^{-n}$ M with $n = 3, 4, 5, 6, 7$. The temperature is of 23 degrees Celsius. The external torque is zero. The circles, squares, and triangles gives the results of the numerical simulations and the solid lines the corresponding fit by Eq. (30). The concentrations are in mole per liter.

Positive values of the external torque can also be considered. In Fig. 12, the mean rotation rate is seen to increase after a minimum. In this case, a tilting of the free-energy potentials is also induced by the external torque as seen in Fig. 13 (a) and (b). Here, the tilting is in the direction of the mean rotation although it was in the opposite direction for negative external torques. The minimum in the rotation rate around $\tau_{\mathrm{ext}} \simeq 35$ pN nm is due to the loss of coincidence between the potential wells and the angles where the transition rates are maximum, because of the external torque. As a consequence, the transition to the next chemical state is hindered and the rotation slowed down. For $\tau_{\mathrm{ext}} > 35$ pN nm, the potentials $U_\sigma(\theta) - \tau_{\mathrm{ext}}\theta$ with $\sigma = 2, 4, 6$ no longer have any barrier opposing the rotation of the γ-shaft, which therefore increases.

In Figs. 11 and 12, we notice that the features in the rotation and ATP synthesis rates appear more or less symmetrically with respect to zero external torque. The reason is that both the features at the stalling torque around $\tau_{\mathrm{ext}} \simeq -35$ pN nm and at the onset of faster rotation around $\tau_{\mathrm{ext}} \simeq +35$ pN nm have a similar origin. Beyond these critical values for $|\tau_{\mathrm{ext}}| > 35$ pN nm, the potentials $U_\sigma(\theta) - \tau_{\mathrm{ext}}\theta$ with $\sigma = 2, 4, 6$ are so tilted that they no longer oppose barriers to the quasi free rotation in the direction of the external torque, as seen in Fig. 13. We also notice that the stalling torque is of the order of the most negative slope of the potentials responsible for the power stroke after ATP binding. Similarly, the positive external torque at the onset of faster rotation around $\tau_{\mathrm{ext}} \simeq +35$ pN nm is of the order of the most positive slope of the same potentials on the other side of their minima. Therefore, the plot of the mean rotation rate versus the external torque is able to reveal these major features of the aforementioned potentials. This could constitute the basis of a method to obtain these potentials by inversion of experimental data.

Furthermore, we observe in Fig. 12 that features appear in the rate of ATP synthesis, which correspond to those of Fig. 11. On the one hand, ATP hydrolysis is much reduced for positive $\tau_{\mathrm{ext}} > +35$ pN nm since the rotation is essentially driven by the external torque and no longer needs ATP consuming reactions. In this regime, the rotation proceeds quasi freely in the potentials $U_\sigma(\theta) - \tau_{\mathrm{ext}}\theta$ with $\sigma = 2, 4, 6$ which no longer have any barrier. On the other hand, for negative τ_{ext} lower than the stalling torque, ATP synthesis saturates at the rate of about 50 ATP/s, without significant dependence on the external torque if this latter is negative enough. In this case, we see in Fig. 11 that the rotation speeds up in the direction of the negative external torque, although the rate of ATP synthesis saturates.

The efficiency of the coupling between the chemistry and the mechanics of the $\mathrm{F_1}$ motor can be characterized by the ratio of the mean rate of ATP synthesis over the mean rotation rate. This ratio gives the mean number of ATP molecules which are hydrolysed or synthesized per revolution. This ratio is obtained by dividing minus the rate of ATP synthesis depicted in Fig. 12 by the rotation rate of Fig. 11 and it behaves accordingly. An example of this efficiency is depicted in Fig. 14 versus the external torque. For an external torque between the stalling torque and the onset of faster rotation, the motor consumes about three ATP molecules per revolution as expected since the barrel contains three β subunits, each one with a catalytic site. In this range of external torques, the coupling between chemistry and mechanics is thus tight. In contrast, the efficiency drops to lower values outside this range.

Above the onset of faster rotation for positive $\tau_{\mathrm{ext}} > +35$ pN nm, this drop is explained by the disappearance of

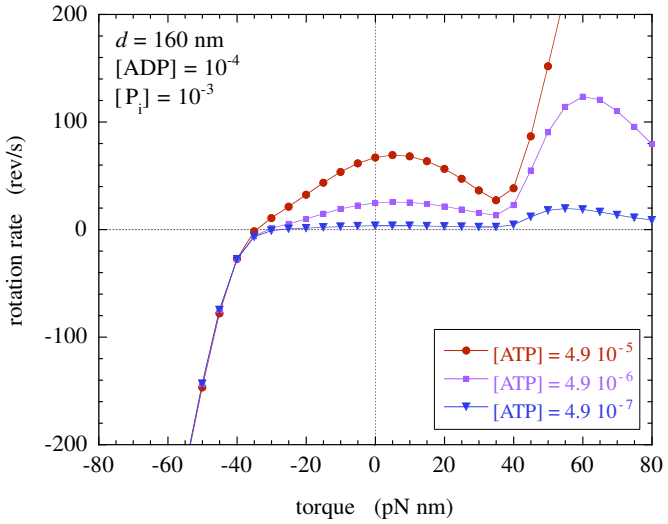

FIG. 11: The mean rotation rate V in revolutions per second versus the external torque $\tau_{\rm ext}$. The diameter of the bead is $d = 160$ nm. The concentrations of the chemical species are [ADP] $= 10^{-4}$ M, [P_i] $= 10^{-3}$ M, and [ATP] $= 4.9\ 10^{-n}$ M with $n = 5, 6, 7$. We notice that the equilibrium state corresponds to $n = 13$. The temperature is of 23 degrees Celsius. The concentrations are in mole per liter.

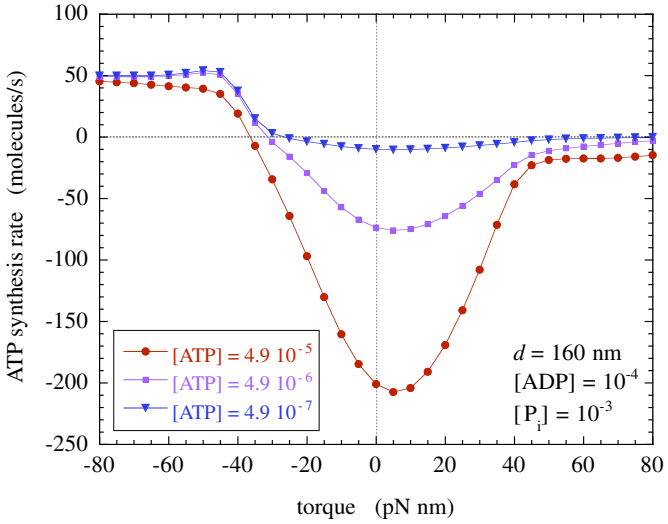

FIG. 12: The mean rate of ATP synthesis in molecules per second versus the external torque $\tau_{\rm ext}$ in the same conditions as in Fig. 11. The diameter of the bead is $d = 160$ nm. The concentrations of the chemical species are [ADP] $= 10^{-4}$ M, [P_i] $= 10^{-3}$ M, and [ATP] $= 4.9\ 10^{-n}$ M with $n = 5, 6, 7$. The temperature is of 23 degrees Celsius. The concentrations are in mole per liter.

barriers in the potentials $U_\sigma(\theta) - \tau_{\rm ext}\theta$ with $\sigma = 2, 4, 6$, so that the rotation proceeds quasi freely in the direction of the external torque without the need of much ATP consumption.

Below the stalling torque for negative $\tau_{\rm ext} < \tau_{\rm ext,stall}$, Figs. 11 and 12 show that both the rotation rate and the rate of ATP consumption become negative so that the efficiency concerns ATP synthesis. In this regime, the number of ATP molecules which are synthesized per revolution by the motor decreases from a value close to three down to smaller values. This is explained because the rotation speeds up while the rate of ATP synthesis saturates around 50 ATP/s. Therefore, ATP synthesis continues to be effective eventhough the efficiency measured in ATP/rev appears to drop. The behavior of the efficiency predicted by the model is consistent with the experimental results of Ref. [17] where ATP synthesis is induced by a rotating magnetic field acting on the gold bead and driving the rotation of the γ-shaft. The experimental value reported in Ref. [17] is of 5 ATP/s at the rotation of 3 Hz, which gives an efficiency of 1.7 ATP/rev below the maximum value of 3 ATP/rev. This corresponds in the present model to a driving slightly

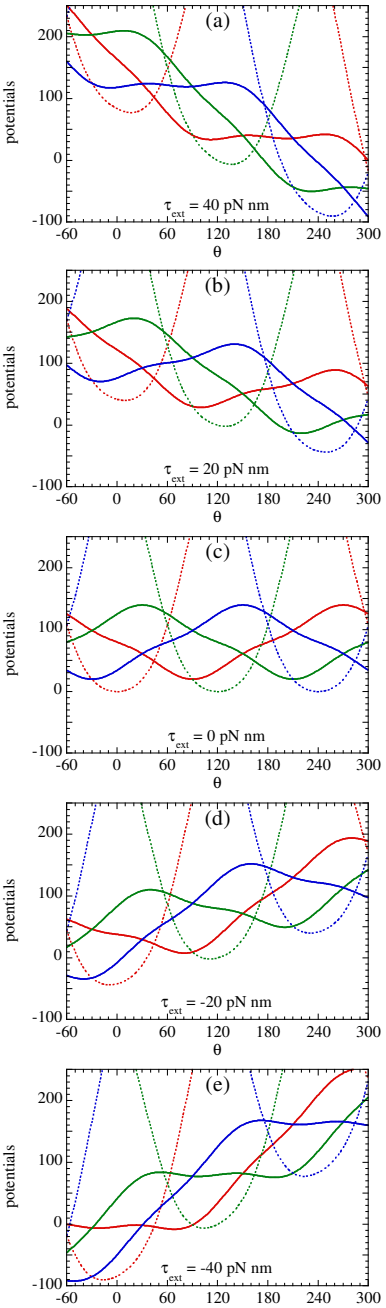

FIG. 13: The free-energy potentials $U_\sigma(\theta) - \tau_{\rm ext}\theta$ of the six chemical states $\sigma = 1, 2, ..., 6$ versus the angle θ, for positive and negative values of the external torque $\tau_{\rm ext}$.

below the stalling torque where the rates of rotation and ATP synthesis take these small values. We notice that ATP synthesis is only possible below the stalling torque where the efficiency is thus necessarily lower than the maximum value of 3 ATP/rev. This maximum efficiency can only reached in the limit where the external torque becomes equal to the stalling torque where the rotation rate vanishes.

Therefore, the mechanism of coupling between the flux of ATP molecules and the rotation of the motor shaft is tight in the range $\tau_{\rm ext,stall} < \tau_{\rm ext} < +35$ pN nm, but loose outside this range [18]. This result has biological significance concerning the coupling with the F_o part in F_oF_1-ATPase. It means that biological evolution should have led to a F_o part able to drive the rotation of the F_1 part with a torque which is large enough to overcome the stalling torque but sufficiently low for the efficiency to remain significant.

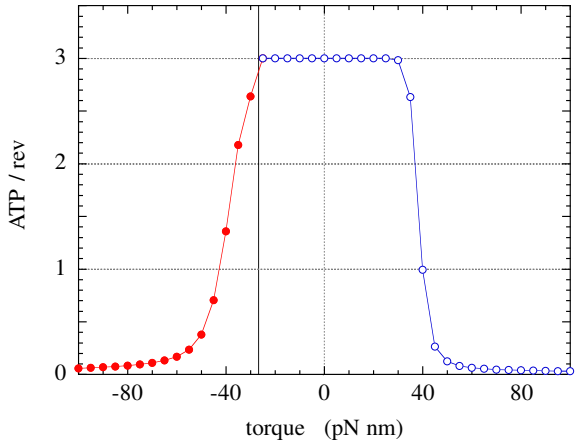

FIG. 14: The mean number of ATP molecules which are consumed or synthesized per revolution versus the external torque $\tau_{\rm ext}$. This number is given by taking the ratio of the ATP synthesis rate in Fig. 12 over the mean rotation rate in Fig. 11 for $[{\rm ATP}] = 4.9\ 10^{-7}$ M. The diameter of the bead is $d = 160$ nm. The concentrations of the other species are $[{\rm ADP}] = 10^{-4}$ M and $[{\rm P_i}] = 10^{-3}$ M. The vertical solid line is located at the stalling torque $\tau_{\rm ext,stall} \simeq -26$ pN nm between the regimes of ATP synthesis on its left-hand side and of ATP hydrolysis on its right-hand side. The temperature is of 23 degrees Celsius.

VII. CONCLUSIONS

In the present paper, we have addressed several important issues concerning the behavior of the F_1-ATPase molecular rotary motor, in particular, under the effects of temperature and external torque.

The vehicle of our study is a stochastic model built on the basis of the experimental observations of Ref. [6]. The random variables of the model are the continuous angle of rotation of the γ-shaft of the motor and the discrete chemical state of its barrel composed of the $(\alpha\beta)_3$ hexamer. Out of the 64 states of the detailed model by Oster and coworkers [8–10], our model retains six chemical states corresponding to the successive occupations and evacuations of the three catalytic sites in each β subunits by ATP or the products ADP and P_i of ATP hydrolysis. The jumps between these six chemical states are the substeps in the rotation of the motor as experimentally observed in Ref. [6] and which are due to the reactions of ATP binding and of the release of the products. The stochastic process of the model is ruled by six coupled Fokker-Planck equations, which can be conceived as coupled diffusion-reaction equations. Here, diffusion refers to the biased Brownian rotation of the γ-shaft in each free-energy potential corresponding to one of the six chemical states and reaction to the random jumps between these chemical states. The free-energy potentials have been fitted to the experimental data of Ref. [6] thanks to the fluctuations of the angle in the potential wells. The modeling shows the equal importance of the transition states of the reactions, which also depend on the angle. In this respect, Arrhenius' law of kinetics has been used, which leads to a model able to make predictions over a whole range of temperatures and which is no longer restricted to a single temperature.

First of all, the model nicely reproduces the main experimental observations reported in Ref. [6]. In particular, the model simulates realistic stochastic trajectories showing not only the steps but also the substeps which have been experimentally observed in Ref. [6]. Furthermore, several key features of the F_1 motor are well described such as the Michaelis-Menten kinetics for the mean rotation rate versus the ATP concentration. The transition of the Michaelis-Menten kinetics occurs between the regime at low ATP concentration where the motor spends most of its time waiting for ATP binding around the angles $\theta = 0°$, 120°, and 240° before the 80°-90° substeps and the regime at high ATP concentration where the motor is mainly waiting for the release of ADP and P_i around the angles $\theta = 90°$, 210°, and 330° before the 40°-30° substeps.

Moreover, the model allows us to understand an important feature in the dependence of the mean rotation rate versus the friction coefficient. This dependence shows a transition between what we call the reaction-limited and the friction-limited regimes. The reaction-limited regime occurs at low friction where the motor spends most of its time waiting for the next reactive event, while fluctuating near the bottom of one of the free-energy potential wells. In this regime, the friction is sufficiently low that the rotation of the shaft just after each reactive event is faster than the waiting time between the reactive events so that the steps and substeps are resolved as it is the case in the experiments of Ref. [6]. On the other hand, in the friction-limited regime, the friction is so high that the rotation can be of the same order as or longer than the characteristic times of the reactions so that the substeps and steps are blurred, as in the early experiments on this motor [5].

Besides, we show that the rotation of the motor is hindered at high concentrations of the products ADP and P_i of

ATP hydrolysis and we propose the simple analytic expression (30) to explain the results of the numerical simulation in some range of validity.

This study leads to several important predictions.

Concerning the dependence on temperature, our model is consistent with Arrhenius' law of chemical kinetics since all its activation energies are non negative. Arrhenius' law means that the reactions with a nonvanishing energy barrier are thermally activated. The activation energies are determined by six potentials for the six transition states connecting the six chemical states. These transition-state potentials depend on the angle of the γ-shaft and their minima are located at the gates of the reactions of ATP binding and product release. With the constraints that the activation energies are non negative, the model predicts that the mean rotation rate increases with temperature following an Arrhenius behavior.

The model also predicts the effects of an external torque have on the F_1 motor. Important features have been identified in the dependences on the external torque of the mean rates of rotation and ATP synthesis.

At positive external torque in the direction of the mean rotation, an onset of faster rotation is predicted following a minimum. This is attributed to the tilting of the free-energy potentials due to the external torque. Beyond some value of the external torque, the tilted potentials no longer present any barrier to the rotation. Therefore, rotation is driven by the external torque and proceeds quasi freely without the need of ATP consumption.

At negative external torque opposing the rotation, the mean rotation rate vanishes at the stalling torque. Below this value, the potentials are also tilted but in the opposite direction. The barriers opposing the free rotation also disappear so that rotation speeds up as the external torque becomes more negative. In this regime, ATP synthesis is driven by the external torque. Although rotation speeds up, the rate of ATP synthesis saturates around 50 ATP/s.

The efficiency of the coupling between the chemistry and mechanics of the motor can be characterized in terms of the mean number of ATP molecules consumed or synthesized during one revolution. The efficiency is measured in ATP/rev and can be calculated as the ratio between the rates of ATP synthesis in ATP/s and rotation in rev/s.

If the external torque belongs to the range between the stalling torque and the onset of faster rotation, the efficiency takes its maximum possible value of 3 ATP/rev. In this range, the coupling is tight between the chemistry and mechanics of the F_1 motor. However, the efficiency drops below the maximum value outside this range for the reason that the potentials responsible for the power strokes of the motor are so tilted by the external torque that they no longer oppose barriers to the quasi free rotation of the γ-shaft. Hence, the rotation rate increases and the efficiency drops. Our prediction is consistent with the observation of the efficiency of 1.7 ATP/rev observed in the experiments of Ref. [17] on ATP synthesis in F_1-ATPase driven by a rotating external magnetic field. We can interpret this drop of the efficiency as a constraint on the torque developed by the F_o part in order for the complete F_oF_1-ATPase to acquire its functionality of ATP synthase during biological evolution.

In conclusion, our results show that the F_1 motor works with a tight chemomechanical coupling for an external torque ranging between the stalling torque and the onset of faster rotation, and by a loose coupling outside this range [18]. Therefore, the coupling mechanism between chemistry and mechanics depends on the working conditions of the motor, in particular, on the external torque. The present model is thus able to bring a unified understanding of many of the experimental observations on the F_1 motor. In regard of the current state of the art, the model provides a good compromise between simplicity and realism. Thanks to this model, we can also investigate the nonequilibrium thermodynamic properties of the F_1-ATPase molecular motor and, in particular, the consequences of the fluctuation theorem [22, 23]. We hope to report on these issues in a future publication.

Acknowledgments. The Authors thank Professor K. Kinosita Jr. for several discussions, as well as Professor S. Tasaki for his hospitality at Waseda University. The Authors are grateful to D. Andrieux for his helpful comments. E. Gerritsma is financially supported by the "Fonds pour la Formation à la Recherche dans l'Industrie et l'Agriculture" (F. R. I. A. Belgium). This research is financially supported by the "Communauté française de Belgique" (contract "Actions de Recherche Concertées" No. 04/09-312) and the National Fund for Scientific Research (F. N. R. S. Belgium, contract F. R. F. C. No. 2.4577.04).

APPENDIX A: DETAILED BALANCE AT EQUILIBRIUM

In this Appendix, we show that the model (13)-(14) with Eqs. (11) and (19)-(22) satisfies the principle of detailed balance at equilibrium. According to this principle, the probability currents vanish between any mesoscopic states in the state of thermodynamic equilibrium. This concerns the stochastic motion on each potential surface as well as the reactions. Accordingly, the probability currents densities (11) vanish at equilibrium, $J_{\sigma,\mathrm{eq}} = 0$, which implies that the probability densities become the equilibrium Boltzmann distributions corresponding to the free-energy potentials:

$$p_{\sigma,\mathrm{eq}}(\theta) \sim \exp\left[-\frac{U_\sigma(\theta) - \tau_{\mathrm{ext}}\theta}{k_{\mathrm{B}}T}\right] \tag{A1}$$

with $\sigma = 1, 2, ..., 6$. The relative values of the six normalizing constants are determined by the conditions of detailed balance for the reactions:

$$W_+\left(\theta - \frac{2\pi i}{3}\right) p_{2i+1,\mathrm{eq}}(\theta) \;=\; W_-\left(\theta - \frac{2\pi i}{3}\right) p_{2i+2,\mathrm{eq}}(\theta) \tag{A2}$$

$$\tilde{W}_+\left(\theta - \frac{2\pi i}{3}\right) p_{2i+1,\mathrm{eq}}(\theta) \;=\; \tilde{W}_-\left(\theta - \frac{2\pi i}{3}\right) p_{2i,\mathrm{eq}}(\theta) \tag{A3}$$

with $i = 0, 1, 2$. We can verify that the detailed balance conditions (A2) and (A3) are indeed satisfied by the transition rates (19)-(22) with the equilibrium Boltzmann distributions (A1) for their dependence on the angle θ. Furthermore, the product over the motor cycle of the ratios of the probability densities is equal to unity:

$$1 = \prod_{\sigma=1}^{6} \frac{p_{\sigma,\mathrm{eq}}(\theta)}{p_{\sigma-1,\mathrm{eq}}(\theta)} = \prod_{i=0}^{2} \frac{\tilde{W}_+\left(\theta - \frac{2\pi i}{3}\right) W_+\left(\theta - \frac{2\pi i}{3}\right)}{\tilde{W}_-\left(\theta - \frac{2\pi i}{3}\right) W_-\left(\theta - \frac{2\pi i}{3}\right)} = \left\{ \frac{[\mathrm{ATP}]_{\mathrm{eq}}}{[\mathrm{ADP}]_{\mathrm{eq}}[\mathrm{P_i}]_{\mathrm{eq}}}\, \mathrm{e}^{-\beta \Delta G^0} \right\}^3 \tag{A4}$$

with

$$\Delta G^0 = G^0_{\mathrm{ADP}} + G^0_{\mathrm{P_i}} - G^0_{\mathrm{ATP}} = -50 \text{ pN nm} \tag{A5}$$

Accordingly, we recover the relation (2) between the equilibrium concentrations if the difference of reference free energies in the right-hand side of Eq. (A5) is equal to the equilibrium Gibbs free energy of hydrolysis. This condition is indeed satisfied for the values of the reference free energies given in Table II. In this way, the principle of detailed balance is verified at equilibrium for both the mechanics and the chemistry of the molecular motor.

APPENDIX B: METHOD OF STOCHASTIC SIMULATIONS

The random time evolution of the molecular motor is simulated thanks to Gillespie's numerical algorithm [14–16]. The continuous angle $0 \leq \theta < 2\pi$ is discretized into $N = 100$ states corresponding to the angles $\theta_l = l\Delta\theta$ with $l = 0, 1, 2, ..., N-1$. This converts the process described by the coupled Fokker-Planck equations (10) into a continuous-time jump process between the $6N$ states (θ_l, σ) with $\sigma = 1, 2, ..., 6$. From each state, four transitions are possible which are the forward and backward motions of the angle $(\theta, \sigma) \to (\theta \pm \Delta\theta, \sigma)$ and the jumps to the neighboring chemical states $(\theta, \sigma) \to (\theta, \sigma \pm 1)$. A transition rate $W_j(\theta, \sigma)$ is associated with each one of these four transitions $j = 1, 2, 3, 4$. The transition rates of the forward and backward motions are given by [16]:

$$W\left[(\theta, \sigma) \to (\theta \pm \Delta\theta, \sigma)\right] = \frac{D}{\Delta\theta^2} \frac{\beta\, \Delta U_{\sigma,\pm}}{\mathrm{e}^{\beta\, \Delta U_{\sigma,\pm}} - 1} \tag{B1}$$

where

$$\Delta U_{\sigma,\pm} = U_\sigma(\theta \pm \Delta\theta) - U_\sigma(\theta) \mp \tau_{\mathrm{ext}} \Delta\theta \tag{B2}$$

D is the diffusion coefficient and $\beta = (k_{\mathrm{B}}T)^{-1}$. The transition rates of the two reactive jumps from a given chemical state σ are given in terms of the transition rates (19)-(22) according to Table I. In the preamble of the simulation, these $24N$ transition rates $W_j(\theta, \sigma)$ are computed for the four possible transitions $j = 1, 2, 3, 4$ of the $6N$ possible states (θ, σ), as well as the cumulative coefficients

$$c_k = \frac{1}{c_0} \sum_{j=1}^{k} W_j(\theta, \sigma) \qquad \text{with} \quad c_0 = \sum_{j=1}^{4} W_j(\theta, \sigma) \tag{B3}$$

The random trajectories are simulated as follows. Starting the some initial state (θ, σ) at time t, two random numbers, r_1 and r_2, are generated which are uniformly distributed in the unit interval. They are used as follows. First, the time interval before the next jump is given by

$$\Delta t = -\frac{1}{c_0} \ln r_1 \tag{B4}$$

Secondly, the next state is the one reached by the transition k if $c_{k-1} < r_2 < c_k$. The system is updated according to

$$t \;\to\; t + \Delta t \tag{B5}$$

$$(\theta, \sigma) \;\to\; (\theta', \sigma') \tag{B6}$$

All the operations are repeated until the final time.

---

[1] B. Alberts, D. Bray, A. Johnson, J. Lewis, M. Raff, K. Roberts, and P. Walter, *Essential Cell Biology* (Garland Publishing, New York, 1998).
[2] P. Mitchell, Nature **191**, 144 (1961).
[3] J. P. Abrahams, A. G. W. Leslie, R. Lutter, and J. E. Walker, Nature **370**, 621 (1994).
[4] P. Boyer, Biochim. Biophys. Acta **1140**, 215 (1993).
[5] H. Noji, R. Yasuda, M. Yoshida, and K. Kinosita Jr., Nature **386**, 299 (1997).
[6] R. Yasuda, H. Noji, M. Yoshida, K. Kinosita Jr., and H. Itoh, Nature **410**, 898 (2001).
[7] K. Shimabukuro, R. Yasuda, E. Muneyuki, K. Y. Hara, K. Kinosita Jr., and M. Yoshida, Proc. Natl. Acad. Sci. U. S. A. **100**, 14731 (2003).
[8] H. Wang and G. Oster, Nature **396**, 279 (1998).
[9] G. Oster and H. Wang, Biochim. Biophys. Acta **1458**, 482 (2000).
[10] S. X. Sun, H. Wang, and G. Oster, Biophys. J. **86**, 1373 (2004).
[11] M. S. Liu, B. D. Todd, and R. J. Sadus, J. Chem. Phys. **118**, 9890 (2003).
[12] Y. Q. Gao, W. Yang, R. A. Marcus, and M. Karplus, Proc. Natl. Acad. Sci. U. S. A. **100**, 11339 (2003).
[13] F. Jülicher, A. Ajdari, and J. Prost, Rev. Mod. Phys. **69**, 1269 (1997).
[14] D. T. Gillespie, J. Comput. Phys. **22**, 403 (1976).
[15] D. T. Gillespie, J. Phys. Chem. **81**, 2340 (1977).
[16] H. Wang, C. S. Peskin, and T. C. Elston, J. Theor. Biol. **221**, 491 (2003).
[17] H. Itoh, A. Takahashi, K. Adachi, H. Noji, R. Yasuda, M. Yoshida, and K. Kinosita Jr., Nature **427**, 465 (2004).
[18] F. Oosawa and S. Hayashi, Adv. Biophys. **22**, 151 (1986).
[19] N. Sakaki, R. Shimo-Kon, K. Adachi, H. Itoh, S. Furuike, E. Muneyuki, M. Yoshida, and K. Kinosita Jr., Biophys. J. **88**, 2047 (2005).
[20] K. Kinosita Jr., K. Adachi, and H. Itoh, Annu. Rev. Biophys. Biomol. Struct. **33**, 245 (2004).
[21] A. J. Hunt, F. Gittes, and J. Howard, Biophys. J. **67**, 766 (1994).
[22] U. Seifert, Europhys. Lett. **70**, 36 (2005).
[23] D. Andrieux and P. Gaspard, Phys. Rev. E **74**, 011906 (2006).